


Local wall shear stress measurements with a thin plate submerged in the sublayer in wall turbulent flows

Dan Hua¹  · Hiroki Suzuki¹ · Shinsuke Mochizuki¹

Received: 5 April 2017 / Revised: 7 July 2017 / Accepted: 7 August 2017 / Published online: 24 August 2017
© Springer-Verlag GmbH Germany 2017

Abstract A local wall shear stress measurement technique has been developed using a thin plate, referred to as a sublayer plate which is attached to the wall in the sublayer of a near-wall turbulent flow. The pressure difference between the leading and trailing edges of the plate is correlated to the known wall shear stress obtained in the fully developed turbulent channel flow. The universal calibration curve can be well represented in dimensionless form, and the sensitivity of the proposed method is as high as that of the sublayer fence, even if the sublayer fence is enveloped by the linear sublayer. The results of additional experiments prove that the sublayer plate has fairly good angular resolution in detecting the direction of the local wall shear stress vector.

List of symbols

AR	Aspect ratio of the plate ($=w/l$)
C_f	Local skin friction coefficient
C_p	Pressure coefficient [$=2(P_w - P_{ref})/(\rho U_c^2)$]
D	Diameter of the static pressure tap
H	Channel height
H	Thickness of the sublayer plate
L	Length of the sublayer plate
P_{ref}	Reference wall static pressure at the inlet of channel
P_w	Wall static pressure
U_c	Mean velocity at the centerline in channel flow
W	Width of the sublayer plate
W	Width of the channel
X	Streamwise coordinate
Y	Coordinate normal to the wall

A	Angle of attack of the sublayer plate with respect to the mean flow direction
ν	Kinematic viscosity
ρ	Fluid density
Δx	Gap between the plate and the pressure hole
ΔP	Pressure difference between the leading and trailing edges of the sublayer plate
*+	Physical quantity normalized by the friction velocity and kinematic viscosity

1 Introduction

The local wall shear stress is the most fundamental quantity when discussing the similarity of the turbulence in the wall layer of boundary layer, pipe, and channel flows. Knowledge of the wall shear stress is very important for many technical applications and for understanding all wall-bounded shear flows. In engineering applications, the wall law and the defect law can be extended to more complicated situations, such as flows subjected to pressure gradients or three-dimensional flows. The law of the wall must be validated in terms of the local wall shear stress as determined by a method independent of any similarity assumptions regarding the statistical properties. Therefore, knowledge of the magnitude and direction of the skin friction vector and its distribution over a surface would be useful.

Classical surveys for measuring the local wall shear stress have been proposed and used in several experimental studies on wall turbulence (e.g., Hanratty and Campbell 1983; Winter 1977), and, more recently, Hanratty and Campbell (1983) and Haritonidis (1989) presented review papers. Measurement techniques for the wall shear stress may be divided into a small group of direct methods (the floating element method and oil film interferometry) and a larger group of indirect

✉ Dan Hua
magicpower1001@gmail.com

¹ Graduate School of Yamaguchi University, 2-16-1 Tokiwadai, Ube 755-8611, Japan

methods, which require calibration in well-known flows such as pipe flows or two-dimensional channel flows. The floating element balance, which considers a large area and is very sensitive (allowing small forces to be determined), is probably the oldest method for measuring wall shear stress. The drag balance technique can be applied to strictly limited situations and requires extremely sophisticated treatment (Allen 1976; Osaka et al. 1998). The recently proposed oil film technique has been used in a boundary layer experiment at higher Reynolds numbers (Bandyopadhyay and Weinstein, 1991). This technique requires careful arrangement of optical devices and considerably accurate oil viscosity values in the experimental setup. The Preston tube and the razor blade are simple and easily accessible devices that are applicable to many cases involving a flow over a smooth surface (Preston 1954; Patel 1965). For turbulent boundary layers, the Preston tube is the most commonly used instrument for skin friction measurements. These devices can be used to determine the local wall shear stress based on similarity only in the sublayer. The wall shear stress can be determined using universal calibration curves for a simple circular Preston tube. The accuracy of the Preston tube method is approximately $\pm 3\%$, and Patel (1965) and Hirt et al. (1986) reported obtaining slightly lower accuracy in experiments involving adverse pressure gradients. However, for cases in which the Preston tube is enveloped by a linear sublayer, the stagnation pressure is too low for accurate measurements at relatively low Reynolds numbers. Nowadays, there are some pressure measurement semiconductor devices that can detect small variations in the order of micro-pascal. However, most of these devices require impractical conditions such as small temperature variation in applications to experiment for aircraft or moving vehicles. Sublayer fences generate a difference in pressure between the stagnation pressure in front of the fence and the pressure behind the fence, which enables more accurate pressure measurement if the fence is enveloped by the linear sublayer. However, each device must be customized and calibrated in canonical flows, such as channel or pipe flows. In addition, the sublayer fence is difficult to construct, primarily due to the narrow gap between fence elements and pressure taps (as shown in Fig. 1). As such, the sublayer fence also requires customized sensors. Moreover, calibration curves must be prepared for each fence in canonical flows in which the wall shear stress is already known accurately. The primary disadvantage of the sublayer fence, however, is that universal calibration curves cannot be obtained for sensors fabricated in the laboratory.

Based on the above considerations, we herein propose a local wall shear stress measurement method using a simple device that is broadly accessible and that provides sufficient accuracy even when the device is enveloped by the linear sublayer. The sublayer plate technique is based on the similarity law. The proposed device, which is referred

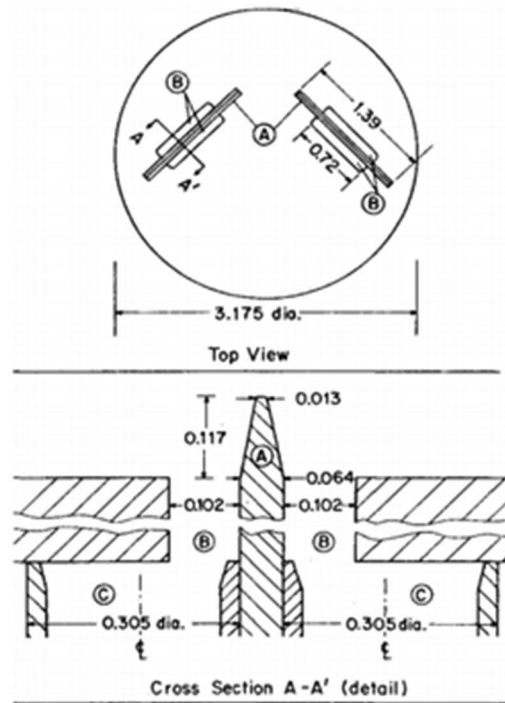
to as a sublayer plate, consists of a thin rectangular plate and two static pressure taps on the wall. The measured differential pressure of the plate is correlated to the local wall shear stress assuming a relationship between this pressure and the velocity distribution close to the wall. In the present study, we experimentally investigate the ability of the sublayer plate to measure the local wall shear stress in a fully developed channel flow. Since the sublayer plate is simple to fabricate, the feasibility of a universal calibration curve is expected to be demonstrated.

2 Experimental device and method

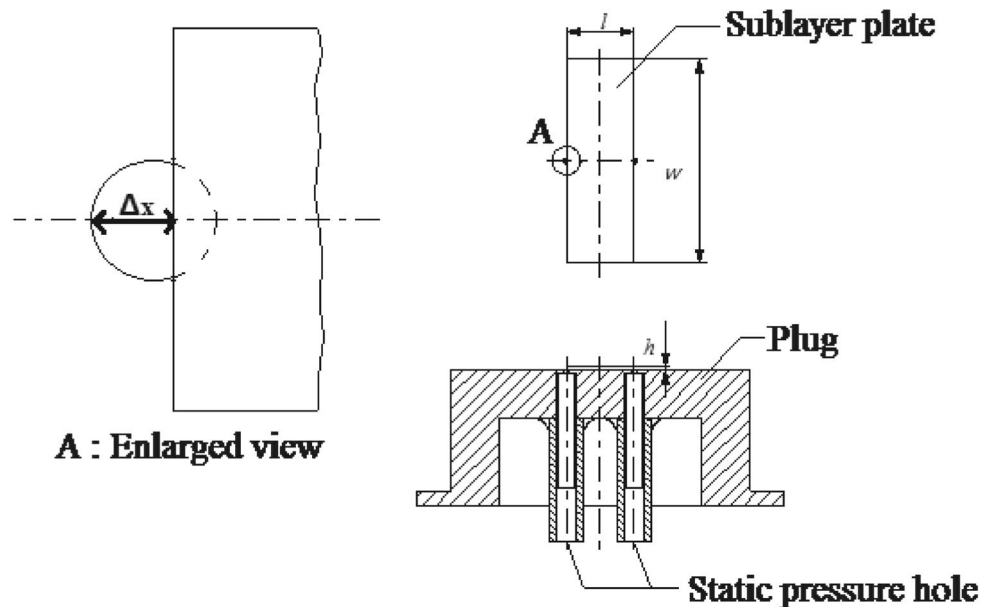
2.1 Sublayer plate

The sublayer plate is a simple, thin, rectangular plate attached to the wall, as shown in Fig. 2. The sublayer plate method is an indirect technique for the measurement of wall shear stress. In this method, a small obstacle is placed on the wall surface, and the difference in pressure is measured and interpreted as shear stress by means of a calibration under known shear stress conditions. The obstacle in the plug is a thin, rectangular plate. And the plug was installed tight with the test wall surface. The protrusion of the plate into the flow (its height above the test surface) was designed as the thickness of the plate. The thickness of the sublayer plate, h , ranges from 0.1 to 0.3 mm. For the channel flow of the present study, these thicknesses correspond to 2.3 to 14.5 times the viscous wall unit. Plates having an aspect ratio, w/l , of 3 for streamwise plate lengths, l , of 5 and 10 mm were used to investigate the angular resolution in Sect. 4.3. The thin plate is made of phosphor bronze and was cut by electric discharge machining. To investigate stagnation at the leading edge and separation at the trailing edge, pressure measurements were conducted using pressure taps of 0.3 mm in diameter situated close to the plate edges. The measured pressure is probably influenced by the relative position of the pressure tap with respect to the plate edge and the open area of the pressure tap. The differential pressure was obtained using a tilt-type manometer. The resolution of the differential pressure was 0.08 Pa. The pressure is slightly reduced if the open area is too small or too large. Some results of the preliminary experiment on the pressure measurement in terms of the gap, Δx , are presented and discussed in Sect. 4.1. The open area of the pressure taps should be independent of the separation and reattachment on the wall. Half of the static pressure tap diameter, $\Delta x = 0.15$ mm, is used as the overlap length in most of the experiments.

Fig. 1 Schematic diagrams of **a** the sublayer fence and **b** the sublayer plate. **a** Top view and cross-section A-A' of the directional surface fence gage (Higuchi 1985). A Fence element, B pressure taps, C stainless steel tunings. Dimensions are in millimeters. **b** Detail of the sublayer plate. A Enlarged view



(a)



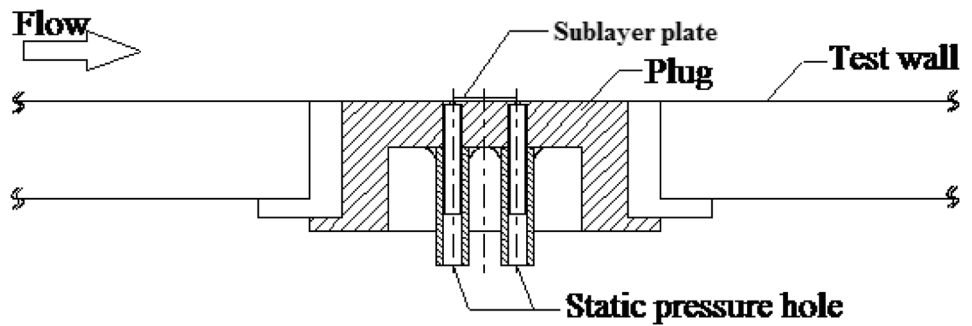
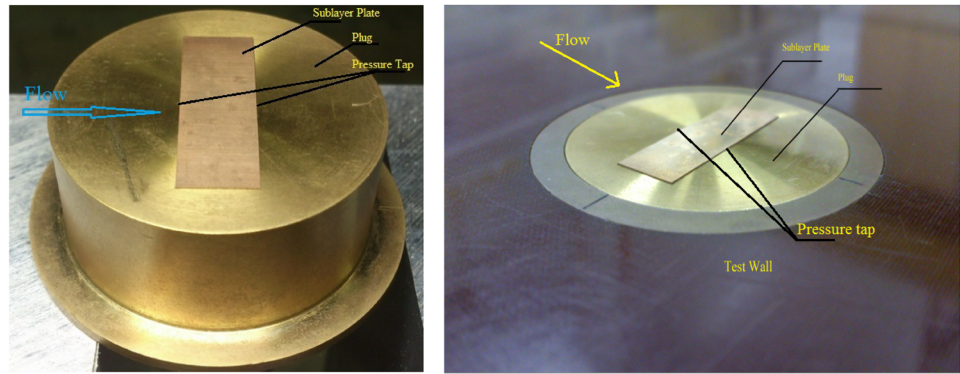
(b)

2.2 Two-dimensional turbulent channel flow

Figure 3 shows a schematic diagram of the flow field and the coordinate system of the channel, the dimensions of which are 700 mm (width) × 40 mm (height) × 6000 mm (length). The

Reynolds number based on the channel center velocity and height $Re = U_C H/\nu$ varied from 8000 to 24,000. The local wall shear stress was determined based on the streamwise gradient of the wall static pressure for the fully developed equilibrium state sufficiently far from the channel entrance. Figure 4

Fig. 2 Photograph of sublayer plate installed in test wall and the sketch of sublayer plate. A bronze plug has 2 small static pressure taps and a rectangular-shaped phosphor bronze plate located on the plug. The longer edges of the plate adjusted to the pressure taps



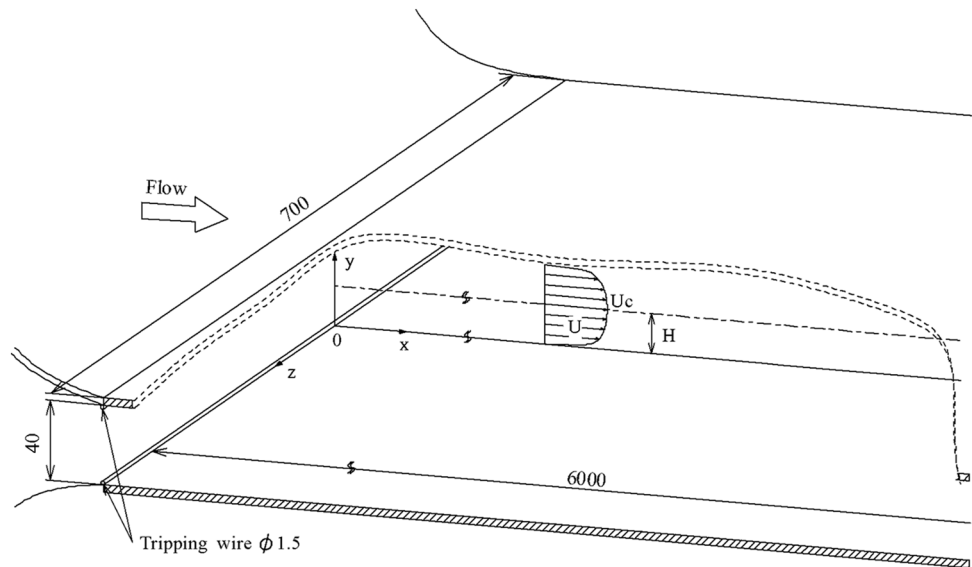
shows that pressure coefficient C_p of wall static pressure is shown against x/H . From the figure, C_p linearly descends with $x/H \geq 56$, indicating that the flow field is the fully developed situation. Figure 5 shows the variation of the local skin friction coefficient as a function of Reynolds number. The experimental results agreed well with the semi-empirical equation proposed by Dean based on a survey of available experimental data (Dean 1978). This agreement appears to be good at higher Reynolds numbers. The result yielded a skin friction coefficient based on the pressure gradient at the surface. For

the turbulent cases, the skin friction coefficient was obtained from measurements of wall static pressure P_w according to the formula as below:

$$\tau_w = -\frac{dP_w}{dx} \frac{H}{2}, \tag{1}$$

$$C_f = \frac{2\tau_w}{\rho U_c^2}. \tag{2}$$

Fig. 3 Schematic diagram of the two-dimensional channel flow, coordinate system, and nomenclature (unit: mm)



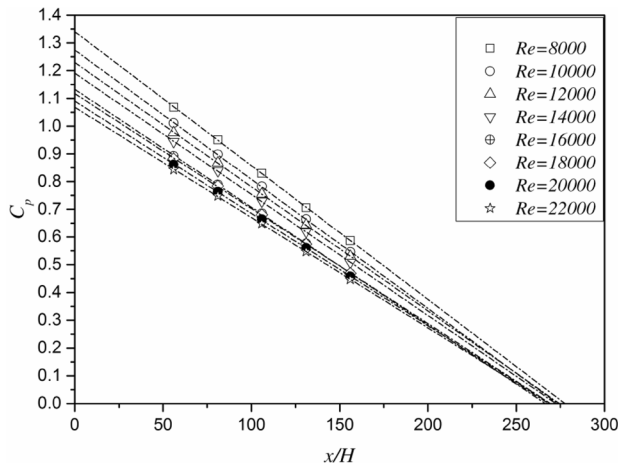


Fig. 4 Wall static pressure distribution in channel flow. Dash dot lines indicate the least-square method with experimental data in the channel flow

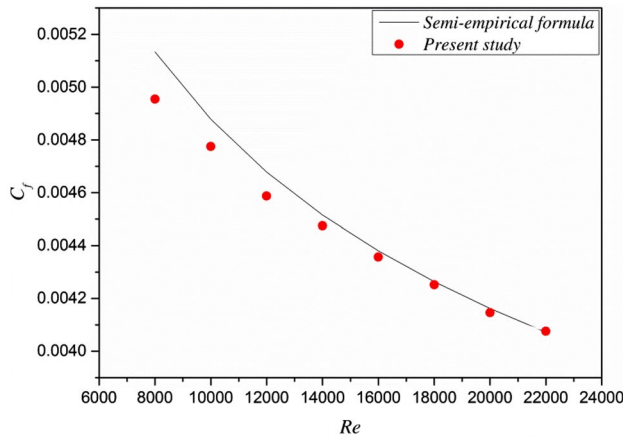


Fig. 5 Variation of the local skin friction coefficient as a function of Reynolds number. The semi-empirical formula is from Dean (1978)

Figure 6 shows that the difference between the data obtained in the present study and Dean’s data. Dean’s equation provides a reliable method for the calculation of the friction coefficient and for the mean velocity distribution over a wide range of Reynolds numbers. For high Reynolds numbers, the percentage error is less than 2%. However, for lower Reynolds numbers, especially at $Re = 8000$, the aspect ratio, which is defined as W/H , might be affected by the non-uniform shear stress around the corners of the plate on the friction law. In the discussion on the magnitude of the Karman constant (Nagib and Chauhan 2008), the uncertainty in the wall shear stress measurements must be less than 2%. Thus, the experimental results for $Re = 8000$ should be disregarded.

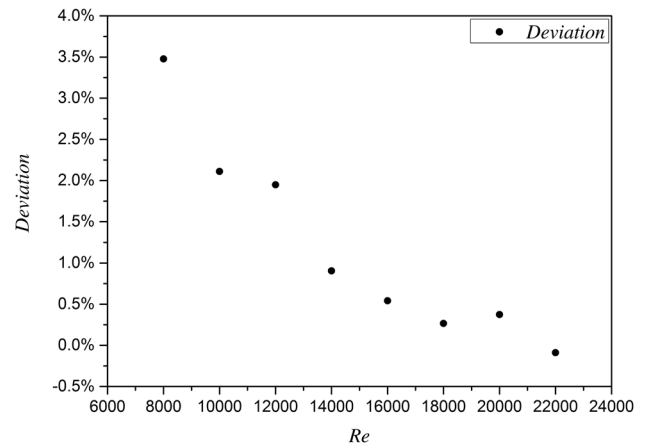


Fig. 6 Deviation between Dean’s data and the data obtained in the experiment of the present study

The logarithmic velocity profiles at downstream positions after a streamwise distance equal to 81 times the channel height ($x = 3240$ mm) as measured from the entrance are given in Fig. 7. We used a microscope with an accuracy of ± 0.005 mm to determine the hot-wire probe origin. Figure 7 shows the comparison of the velocity profile in the present channel flow and the log law. There are many arguments on the standard values involved in the logarithmic law (see e.g. Nagib and Chauhan 2008). For the wall layer expected by the presence of the logarithmic velocity profile in the layer greater than $y^+ = 100$, the velocity profile well agrees with the standard log law. The flow field used in the present experiments is relatively low. The logarithmic velocity profile seems to appear for the narrow layer in Fig. 7. The experimental data show that the present flow field contains the sublayer covered by the wall layer. These experimental facts guarantee that the present channel flow is a suitable one for calibration of the local wall shear stress device. Although the universal value of the Karman constant for a two-dimensional channel flow remains unknown, the experimental data of the present study agree well with the solid line representing the results of a survey conducted by Nagib and Chauhan (2008). The streamwise turbulent intensity profiles are compared to the experimental data at low Reynolds numbers reported by Wei and Willmarth (1989) and Antonia et al. (1992) in Fig. 8. The maximum value of the turbulent intensity is in reasonably good agreement with their experimental data. The measured streamwise mean and turbulent velocities are obtained using a single hot-wire probe and a constant-temperature anemometer. The hot-wire measurement is performed using a tungsten-filament sensor having a diameter of $2.5 \mu\text{m}$ and an active length of 0.5 mm. The active length is less than 20 times the viscous wall unit, that is, spatial resolution of the hot-wire sensor is satisfied for turbulence measurement (Ligrani and Bradshaw 1987).

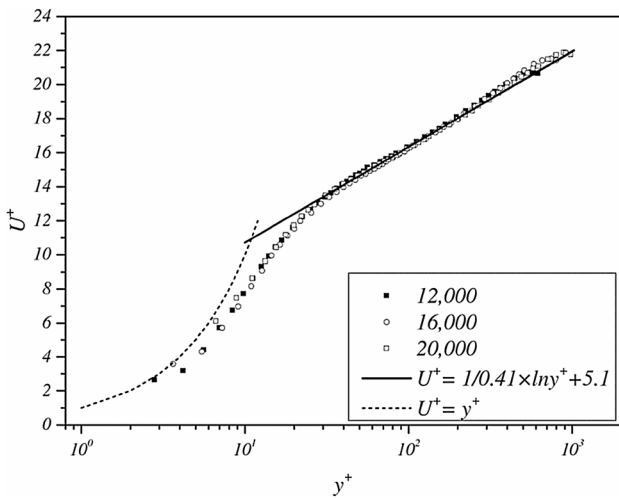


Fig. 7 Log-law profiles at Reynolds numbers of 12,000 (filled square), 16,000 (open circle), and 20,000 (open square). The solid line indicates the log-law profile, and the dashed line indicates the law of the wall in the viscous linear sublayer

3 Results and discussion

3.1 Pressure distributions and calibration curve

The sublayer plate is easier to build than the sublayer fence and requires only a precise manometer to read the pressure difference, ΔP , between upstream and downstream of the plate. To obtain the calibration curve, the correlation

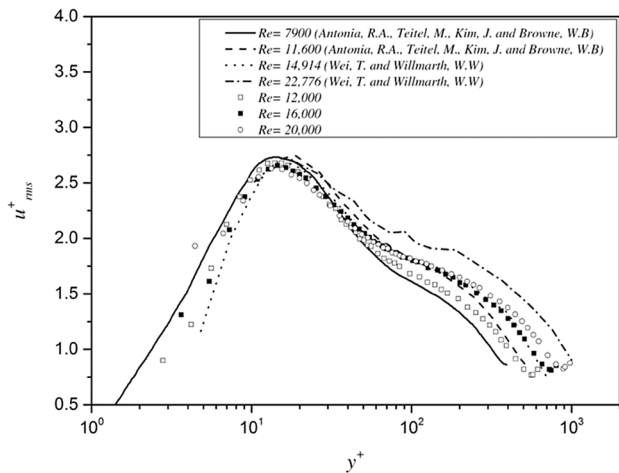


Fig. 8 Experimental and numerical streamwise turbulent intensity profiles obtained in previous channel flow experiments and in the present study at Reynolds numbers of 12,000 (filled square), 16,000 (filled circle), and 20,000 (filled square). The solid and dashed lines indicate the streamwise turbulent intensity profiles calculated by Antonia, R.A., Teitel, M., Kim, J. and Browne, W.B, and the dotted and dash-dotted lines indicate the streamwise turbulent intensity profiles obtained by Wei, T. and Willmarth, W.W

between the pressure difference and the wall shear stress was examined for a plate placed on the wall in the channel flow at a streamwise distance of 81 times the channel height from the entrance. The thickness of the plate was on the same order as the diameter of the static taps in the wall, and separation bubbles were likely to appear in front of and behind the plate. The pressure difference presumably depends on the relative positioning of the plate with respect to the taps. The influence of the relative positioning on the wall pressure measurements was investigated using plates of three thicknesses, namely $h = 0.1, 0.2,$ and 0.3 mm, and the measured static wall pressure is plotted in Fig. 9. In the figure, P is the pressure with the sublayer plate, and P_w is the wall static pressure without the sublayer plate at the same location. Of course, because the pressure and the wall static pressure are not measured at the same time, flow conditions must remain the same for the pressure difference to be valid. The experiments were conducted at $Re = 16,000$, and l was fixed at 10 mm. The plate thicknesses correspond to 3.7, 7.3, and 10.8 times the viscous wall unit for $h = 0.1, 0.2,$ and 0.3 mm, respectively. The stagnation pressure at the leading edge of the plate was relatively high for the thickest plate ($h^+ = 10.8$), where the leading edge was located in the buffer layer. At the trailing edge, the magnitude of the negative pressure for the thinnest plate ($h^+ = 3.7$) was smaller than in the other cases. The thinnest plate was enveloped by a linear sublayer, and the viscous effect appeared to prevent the occurrence of a larger negative pressure at the trailing edge-facing step. The heights of the protrusions on the wall were classified as being fluid-dynamically smooth if the protrusion height was less than five times the viscous wall unit (see, e.g., Schlichting 1979). Based on the experimental results for the cases of $h^+ = 7.3$ and 10.8, the positive pressure at the leading edge and the negative pressure at the trailing edge are approximately independent of the gap, Δx ,

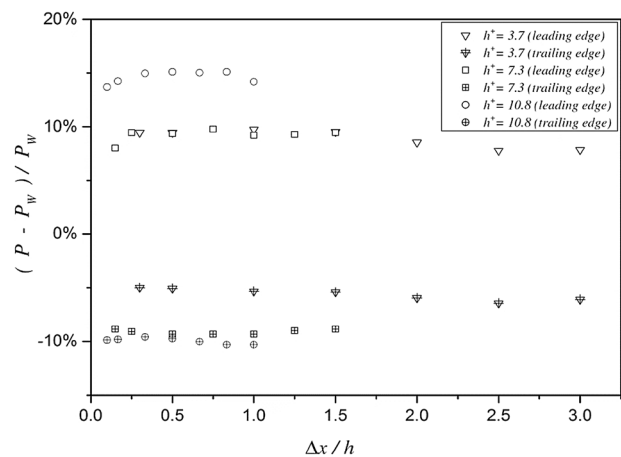


Fig. 9 Static pressure at the leading and trailing edges of the plate as a function of the gap between the plate and the pressure tap

over the range of 0.15 ± 0.05 mm. The static pressure tap should be located in the separation bubble near the leading and trailing edges. In other words, the pressure taps should not be located near the separation and reattachment points on the wall. Otherwise, the relative distance between the tap and the plate edge should not be too small because the static pressure measured through a small tap is influenced by viscosity.

Calibration curves must be determined as the functional relation between two dimensionless quantities derived from dimensional arguments, in a manner similar to that of a Preston tube or a sublayer fence, as follows:

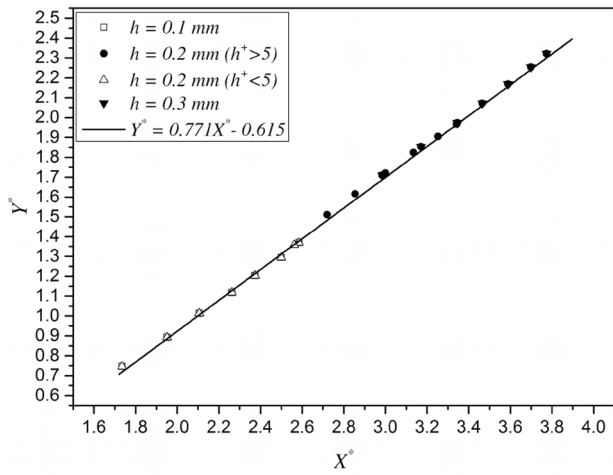
$$Y^* = \log(\tau_w h^2 / \rho v^2) \text{ and } X^* = \log(\Delta P h^2 / \rho v^2). \quad (3)$$

The functional relation between the two dimensionless quantities for three plate thicknesses ($h = 0.1, 0.2,$ and

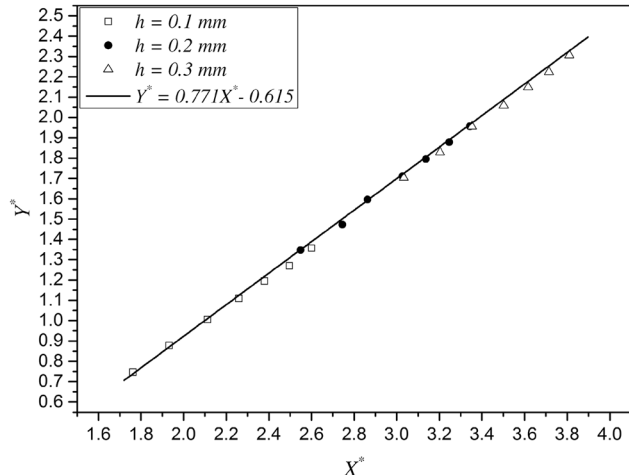
0.3 mm) is plotted for $l = 2, 5$ and 10 mm in Fig. 10. The straight line indicates the relation obtained by the least-squares method for all of the experimental data obtained with sublayer plates of nine sizes for $l = 2, 5$ and 10 mm. All of the experimental results can be well represented by a universal calibration curve calculated by the following equation without any clear differences associated with the thickness and length of the plate:

$$Y^* = 0.771X^* - 0.615 \quad 1.72 < X^* < 3.90 \quad (4)$$

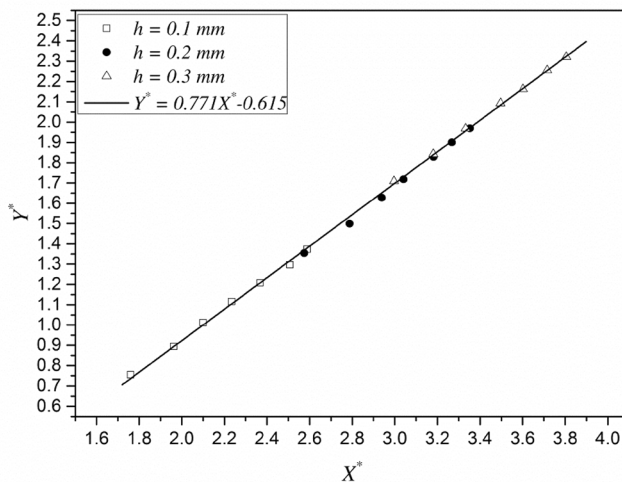
In the previous experiment (Mochizuki et al. 2014), the experimental data were obtained for three thicknesses and $l = 10$ mm. As shown in Fig. 10, for $1.72 < X^* < 2.45$ and $h^+ < 5$, the data in the previous and present experiments well agrees with the solid line plotted by Eq. (4).



(a)



(b)



(c)

Fig. 10 Calibration curve for three parameters obtained from experimental data. **a** $l = 2$ mm, **b** $l = 5$ mm, **c** $l = 10$ mm

Compared to the calibration curve obtained by the sublayer fence (Higuchi 1985) (in the viscous sublayer), the pressure difference normalized by the wall variables obtained from the streamwise pressure gradient in the channel flow is slightly smaller. Figure 11 shows the deviation between the calibration curve and the data obtained in the present study. The maximum deviation between the calibration curve and the data obtained in the present study is less than 1%. Moreover, X^* ranges from 1.72 to 3.90. Figure 11 indicates that as X^* increases, the range of deviations also increases. The curve trend is the most gentle for $l = 2$ mm. The deviation is the smallest for $l = 10$ mm. Although it might appear that the sublayer plate cannot be used to measure the local wall shear stress and has low spatial resolution, the Preston tube requires a longer longitudinal tube length equivalent to 10 times the tube diameter, as well as spanwise separation from the wall static tap. In most flow fields encountered in engineering, 100 times the viscous wall unit is less than 1/100 the boundary layer thickness. The sublayer plate is expected to be able to measure the local wall shear stress for almost the entire range of high-Reynolds-number wall turbulence provided the plate can be manufactured thin enough to remain in the viscous sublayer. To verify the universality of the calibration curve, based on the conclusion from the channel flow, we did the same experiment in a fully developed pipe flow. In the pipe flow, the plate was glued on the surface and the thickness ($h = 0.05$ and 0.1 mm) was measured by a micrometer. The length of the plate is 5 mm. The accuracy of measurement is of the order 1 \AA . The pipe flow having 70 mm diameter and 5700 mm length was confirmed as a standard one in which logarithmic velocity profile with Karman constant 0.41 and additive constant 5.0 (Thuyein

et al. 2010). As shown in Fig. 12, we compared the two types of flow. For $2.3 < X^* < 3.4$, the data from channel flow and pipe flow are agreed well with the calibration curve. It indicates that under the current experimental conditions, the sublayer plate could produce the universal behavior both in channel flow and pipe flow.

In the present study, the sensitivity of the sublayer plate is compared with experimental data (Higuchi 1985 and Rechenberg 1963) reported in a survey by Winter (1977). The sensitivity, which is defined as the ratio of the pressure difference to the wall shear stress, is compared with the sensitivities of the sublayer fence, the Preston tube, and the razor blade methods in Fig. 13. The Preston tube, which uses only the stagnation pressure, has a lower sensitivity at a smaller dimensionless height. At a smaller dimensionless height as compared to the wall, h^+ , the sensitivity of the sublayer plate is as high as that of the sublayer fence. The deviation between sublayer plate and the sublayer fence is less than 2% in the linear sublayer. For both the sublayer fence and the sublayer plate, the use of negative pressure at the trailing edge is advantageous for pressure difference measurement at low Reynolds numbers. The experimental evidence indicates that the sensitivity of the sublayer plate is sufficient if the plate is enveloped by the linear sublayer.

It was unexpected that the sublayer plate has sensitivity as high as the sublayer fence. The fences likely make larger separation bubble and lower pressure behind it. However, the plate has almost same level of sensitivity as the plate and fence are submerged in the linear sublayer. When the edge of the fence and plate are in the buffer layer, the sensitivity of the plate is certainly lower than that of the

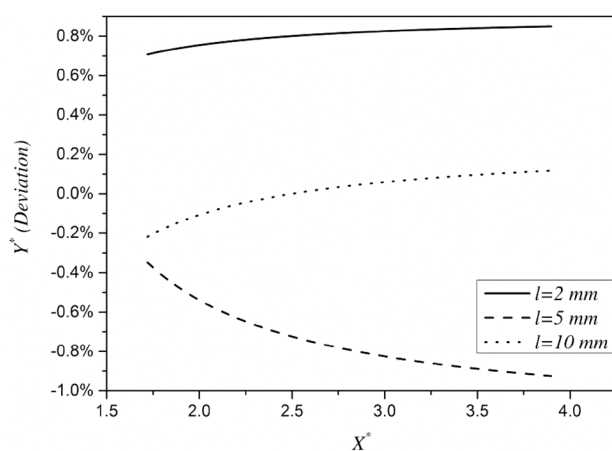


Fig. 11 Percentage deviation of the calibration curve obtained from the experimental data

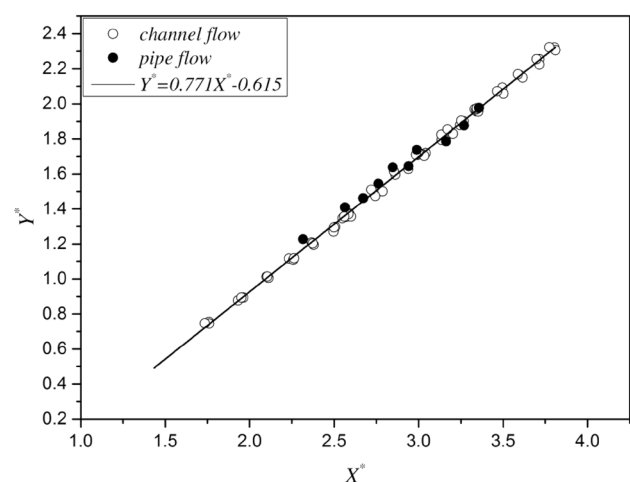


Fig. 12 Universal of the calibration curve for channel flow and pipe flow. The pipe flow is in fully developed condition in which the logarithmic velocity profile with Karman constant of 0.41 and additive constant of 5.0 (Thuyein et al. 2010)

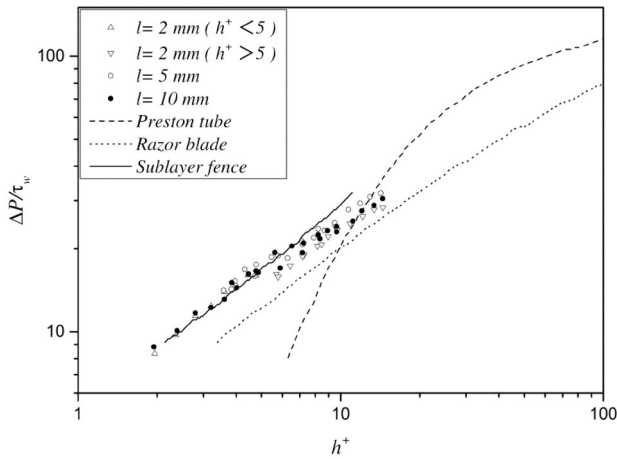


Fig. 13 Sensitivity of the sublayer fence, a razor blade, and a Preston tube. The lines of Preston tube, razor blade and sublayer fence are referred from the review reported by Winter (1977)

fence. The facts suggest that behaviors of separation from edge are similar for the plate and fence if they were submerged in the linear sublayer. The flow is purely viscosity and any obstacles are supposed to be classified as hydrodynamically smooth (see e.g. Schlichting 1979). As the fence and plate are submerged in the linear sublayer, it is fairly expected that the plate and fence can produce the same level of the pressure difference.

3.2 Effect of plate width

The finite spanwise width of the sublayer plate may affect the pressure measurement. The plate length and thickness were fixed at $l = 2$ mm and $h = 0.2$ mm, respectively, and the experiment was conducted at $Re = 16,000$. Four widths, 6, 8, 10, and 13.3 mm, corresponding to aspect ratios of 30, 40, 50, and 66.5, were investigated. Figure 14 shows the dependence on w/h of the measured pressure at the leading and trailing edges. The vertical axis indicates the change in pressure associated with the sublayer plate installation position. In the figure, P is the pressure with the sublayer plate, and P_w is the standard wall static pressure without the sublayer plate. The aspect ratio does not appear to affect the stagnation pressure at the leading edge. When $w/h < 50$, the magnitude of the negative pressure at the trailing edge is reduced to a lower aspect ratio. The sensitivities of these plates are plotted in Fig. 15 in the same manner as in Fig. 13. The narrower plates have slightly lower sensitivity and a lower pressure difference for the same wall shear stress and h^+ . Both edges of the plate usually generate longitudinal vortices, as was often observed in the flow around obstacles placed on the wall. These vortices are referred to as necklace or horseshoe vortices, and the pair of longitudinal vortices induces a

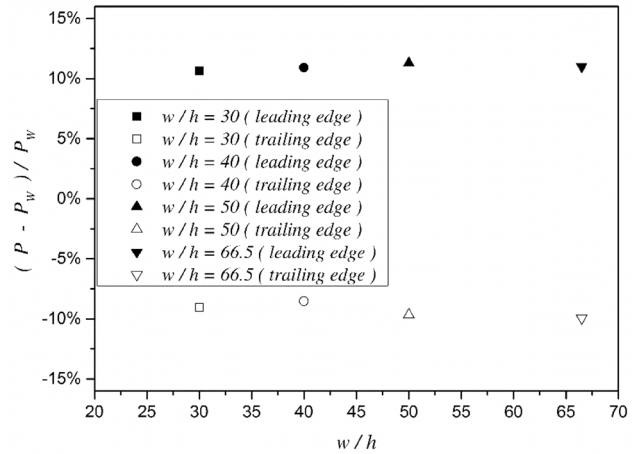


Fig. 14 Effect of plate width on the static pressure at the trailing and leading edges

secondary current toward the wall just downstream of the obstacle (see, e.g., Lugt 1983). The vortices are of the same order as the obstacle height. In the case of an insufficient spanwise width of the plate, the secondary current could reduce the magnitude of the negative pressure at the trailing edge of the plate. For a sufficiently larger spanwise width for $w/h > 50$, the longitudinal vortices do not affect the pressure at the centerline downstream of the obstacle.

3.3 Angular resolution

The sublayer plate produces a stagnation pressure at the straight leading edge, as has been observed for the sublayer fence. The stagnation pressure is expected to depend on the angle of attack of the plate edge with respect to the wall shear stress or limited streamline orientation. This

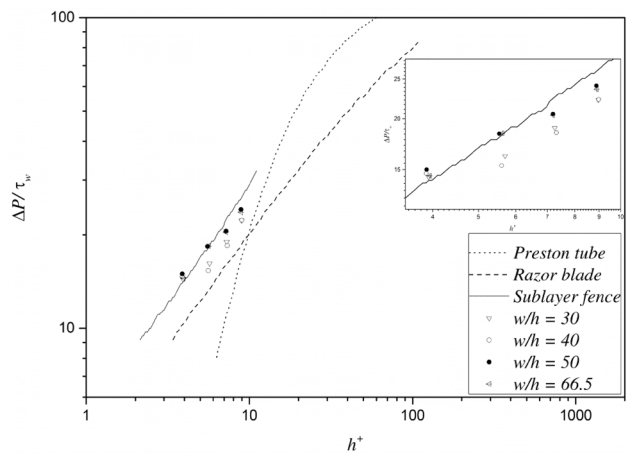


Fig. 15 Effect of plate width on dimensionless pressure sensitivity. Comparison is made in the same manner as in Fig. 13

property could be used to detect the direction of the wall shear stress and limited streamline. The dependence of the pressure difference on the angle of attack of the plate with respect to the wall shear stress was examined experimentally for three plate lengths, $l = 2, 5,$ and 10 mm, and two plate thicknesses, $h = 0.1$ and 0.3 mm. The plate width was maintained at greater than 50 times the plate thickness, and the experiment was conducted at $Re = 16,000$. The angle of attack was varied by rotating the plug on which the sublayer plate was mounted (see Fig. 2). The effect of the aspect ratio on the angular resolution was examined for plate lengths of 5 and 10 mm for $h = 0.2$ mm and $w = 30$ mm, and the obtained results are shown in Fig. 16. The pressure difference was normalized by a pressure difference at an angle of attack, α , of 0 degrees. The solid line represents the semi-empirical relation proposed for the sublayer fence by Vagt and Fernholz (1973):

$$\frac{\Delta P_\alpha}{\Delta P_n} = \exp \left[- \left(1.025 \frac{\pi}{180} \alpha^\circ \right)^2 \right]. \quad (5)$$

The sublayer plate has approximately the same dependence on the stagnation pressure as the semi-empirical relation proposed for the sublayer fence at angles of attack of less than 60° . The experimental data for $AR = 3$ and $AR = 6$ agree well with the sublayer fence up to attack angles of less than 60° (the percentage error less than $\pm 4\%$).

4 Conclusions

A local wall shear stress measurement technique involving a sublayer plate was proposed to determine the local wall

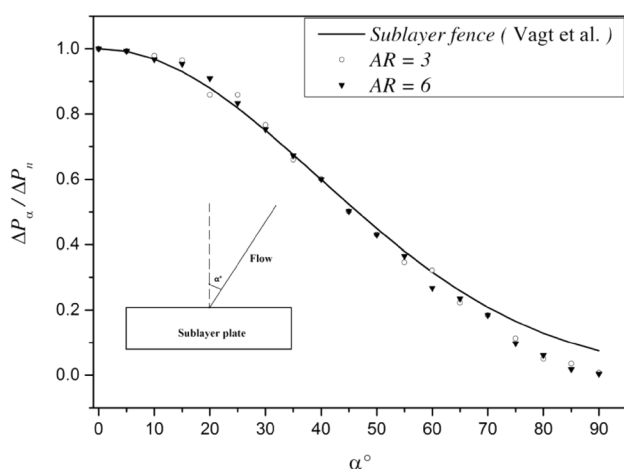


Fig. 16 Variation of pressure difference with yaw angle of attack for aspect ratios of 3 and 6. The solid line represents the semi-empirical formula for the sublayer fence reported by Vagt and Fernholz (1973)

shear stress using an easily fabricated device, and experiments were conducted to investigate the accuracy and angular resolution in a canonical wall turbulent flow, namely a fully developed two-dimensional turbulent channel flow.

The calibration curve generated by the two dimensionless parameters is independent of the specifications of the sublayer plate and is not affected by the finite length of the plate, the streamwise length, or the spanwise width. The sensitivity of the sublayer plate is as high as that of the sublayer fence if they were submerged in the linear sublayer. If the plate is enveloped by the linear sublayer, the sublayer plate can produce a pressure difference sufficient for accurate measurement of the local wall shear stress. The angular resolution of the sublayer plate is represented in the same manner as that of the sublayer fence. It is expected that the sublayer plate can be used to detect the direction of the wall shear stress. Based on the comparison of plates of various sizes, the plate width should be greater than respectively 50 times the thickness of the sublayer plate. Note that, unlike the sublayer fence, the sublayer plate is easily fabricated. A unique calibration curve must be obtained in a canonical flow field for each individual sublayer fence. In contrast, sublayer plates can be used for wall shear stress measurement using a universal calibration curve, as with the Preston tube method.

Acknowledgements This work was supported by JSPS KAKENHI Grant Number 15K13871. We thank Mr. Fukunaga and Mr. Kishii for careful experiment.

References

- Allen JM (1976) Systematic study of error sources in skin friction balance measurements, NASA TN-D-8291
- Antonia RA, Teitel M, Kim J, Browne WB (1992) Low-Reynolds-number effects in a fully developed turbulent channel flow. *J Fluid Mech* 236:579–605
- Bandyopadhyay PR, Weinstein LM (1991) A reflection-type oil-film meter. *Exp Fluids* 11:281–292
- Dean RB (1978) Reynolds number dependence of skin friction and other bulk flow variables in two-dimensional rectangular duct flow. *Trans ASME J Fluids Eng* 100:215–223
- Hanratty TJ, Campbell JA, Goldstein RJ (1983) *Fluid Mechanics Measurements*. Hemisphere Publications, New York, pp 559–615
- Haritonidis JH (1989) The measurement of wall shear stress. In: Gad-el-Hak M (ed) *Advances in Fluid Mechanics Measurements. Lecture Notes in Engineering*, vol 45. Springer, Berlin, Heidelberg, pp 229–261
- Higuchi H (1985) A miniature, directional surface-fence gage. *AIAA J* 23(8):1195–1196
- Hirt F, Zurfluh U, Thomann H (1986) Skin friction balances for large pressure gradients. *Exp Fluids* 4(5):296–300
- Ligrani PM, Bradshaw P (1987) Spatial resolution and measurement of turbulence in the viscous sublayer using subminiature hot-wire probes. *Exp Fluids* 5(6):407–417
- Lugt HJ (1983) *Vortex flow in nature and technology*. University of California, Wiley, pp 85–87

- Mochizuki S, Fukunaga M, Kameda T, Sakurai M (2014) Sublayer plate method for local wall shear stress measurement. In: 19th Australia Fluid Mechanics Conference, Melbourne, Australia, 8–11, Dec, 2014
- Nagib HM, Chauhan KA (2008) Variations of von Karman coefficient in canonical flows. *Phys Fluids* 20(101518):1–10
- Osaka H, Kameda T, Mochizuki S (1998) Re-examination of the Reynolds-number-effect on the mean flow quantities in a smooth turbulent boundary layer. *JSME Int J* 41(1):123–129
- Patel VC (1965) Calibration of the Preston tube and limitations on its use in pressure gradients. *J Fluid Mech* 23(1):185–208
- Preston JH (1954) The determination of turbulent skin friction by means of pitot tubes. *J R Aeronaut Soc* 58:109–121
- Rechenberg I (1963) Messung der turbulenten Wandschubspannung. *Zeitschrift für Flugwissenschaften* 11(11):429–438
- Schlichting H (1979) *Boundary layer theory*, 7th edn. McGraw-Hill, New York, pp 616–617
- Thuyein AW, Mochizuki S, Kameda T (2010) Response of fully developed pipe flow to rough wall disturbances (mean velocity field). *J Fluid Sci Tech* 5(2):340–350
- Vagt JD, Fernholz H (1973) Use of surface fences to measure wall shear stress in three-dimensional boundary layers. *Aeronaut Quart* 24(2):87–91
- Wei T, Willmarth WW (1989) Reynolds-number effects on the structure of a turbulent channel flow. *J Fluid Mech* 204:57–95
- Winter KG (1977) An outline of the technique available for the measurement of skin friction in turbulent boundary layers. *Prog Aerospace Sci* 18(1):1–57